

NOTE: The authors have identified fundamental errors in the following article. We are working on a corrected version, so check back soon.

Towards Online Observability-Aware Trajectory Optimization for Landmark-based Estimators

Kristoffer Frey^{1,2}, Ted Steiner², and Jonathan P. How¹

¹ Massachusetts Institute of Technology, Cambridge MA 02139, USA,
kfrey,jhow@mit.edu

² Charles Stark Draper Laboratory, Cambridge MA 02139, USA,
tsteiner@draper.com

Abstract. As autonomous systems rely increasingly on onboard sensing for localization and perception, the parallel tasks of motion planning and state estimation become increasingly coupled. This coupling is well-captured by augmenting the planning objective with a posterior-covariance penalty – however, online evaluation and optimization can be challenging, particularly for observation models with latent environmental dependencies (e.g., opportunistic landmarks). This paper addresses a number of fundamental challenges in efficient prediction and minimization of the posterior covariance particular to landmark- and SLAM-based estimators. First, we provide a measurement bundling approximation that enables high-rate sensors such as cameras to be approximated with fewer, low-rate updates. This also allows for landmark *marginalization*, for which we provide a novel recipe for computing the gradients necessary for optimization. Finally, we identify a class of measurement models for which the contributions from each landmark can be directly combined, making evaluation of the information gained at each timestep (nearly) independent of the number of landmarks. This opens the door for generalization to landmark *distributions*, foregoing the need for fully-specified linearization points. Taken together, these contributions allow SLAM estimators to be accurately and efficiently approximated, paving the way for online, observability-aware trajectory optimization.

Keywords: observability, belief-space planning, trajectory optimization

1 Introduction

In the last decade, significant progress has been made to enable basic autonomy for low-SWaP (Size, Weight, and Power) systems. Thanks to recent algorithmic advances, such systems can navigate purely from onboard sensors and avoid dependence on dedicated infrastructure such as GPS or motion-capture, allowing operation in a wider range of environments. However, commonly-used sensors such as IMUs, laser scanners, and cameras have nonlinear observation models and/or limited field-of-view (FoV), and therefore the observability of the estimated state depends on the system trajectory. Furthermore, these sensors can have time-varying latent parameters (e.g., IMU biases, rigid-body calibrations)

and environmental dependencies (e.g., the presence or absence of high-gradient corner features). Thus, even with a good initialization point, estimation quality can degrade to catastrophic levels if the chosen trajectory or environment does not provide sufficient information.

In this paper, we are interested in discovering well-observable motions accounting for the (possibly latent) distribution of landmarks over receding time-horizons. This motivates continuous optimization techniques leveraging a full-DoF system model, and efficient evaluation requires a compact representation of the SLAM system. In focusing on receding time-horizons, we are willing to neglect certain aspects of SLAM such as global loop closure in favor of computational efficiency and applicability to real-world scenarios where the map is not fully known at planning time.

When formulating the uncertainty-aware problem, it is common [2, 7, 16, 19, 20, 22] to represent uncertainty via a Gaussian distribution about a nominal linear-time-varying (LTV) trajectory. This representation is deterministic and compactly parameterizable, and is therefore amenable to optimization based on sampling [2, 16, 19], motion-primitives [4, 5, 9, 22], or continuous optimization [7, 20]. Of these, sampling-based approaches are not well-suited for systems with more than a few degrees of freedom, and motion-primitive solutions do not address the fundamental issue of ensuring trajectories are well-observable in the first place. In the space of continuous trajectory optimization, existing approaches have only been demonstrated with relatively simple sensor models [15, 17, 20] or scale poorly with large numbers of landmarks [7].

In order to avoid the computational complexity of explicit covariance minimization, heuristic approaches maximize an observability or (in the case of landmark-based systems) visibility metric. For example, [1, 3, 11] identify and enumerate non-observable trajectories to hand-design a discrete set of “well-observable” maneuvers for use in online planning. More recently, [14] leverages a reinforcement learning framework to select a sequence of primitive maneuvers in a manual calibration routine. From the side of continuous optimization, [10, 15] maximize observability metrics based on the Local Observability Gramian (LOG) in a continuous-optimization setting. For landmark-based systems with limited FoV (e.g., cameras), explicit visibility-based metrics have been used by [6] and [13] in real-time planning frameworks, with some success. However, heuristic methods ultimately fail to capture the full observability characteristics of the system, and therefore may select high-energy (expensive) trajectories with little corresponding estimation improvement [17].

Exact posterior-covariance minimization is challenging for many reasons, particularly in the case of SLAM. As the covariance must be propagated explicitly along the trajectory, the number of updates scales with the measurement rate and can be prohibitive for high-rate sensors such as cameras. Furthermore, landmark-based systems such as visual-SLAM can estimate tens or hundreds of landmarks simultaneously, and linearization points of to-be-discovered landmarks are unknown at planning time. Besides having to compute and accumulate the contribution from each of these landmarks (linear complexity), exact

representation of the joint belief state requires augmenting the covariance matrix with the map uncertainty, an intractable quadratic growth in complexity. While [9] and [4] introduce some sparsification and incremental-update techniques to partially mitigate the cost of evaluation with large maps, they require known landmark linearization points and are applicable only in the case of finite action sets.

1.1 Contributions

In this work, we address these challenges to enable efficient posterior-covariance minimization for a general class of landmark-based observation models.

- **Measurement bundling:** To avoid computing a full estimator update for every measurement timestep, in Section 3 we propose a bundling scheme that allows approximation of high-rate measurements with fewer, low-rate updates.
- **Handling unknown landmarks:** We avoid explicitly augmenting the covariance matrix (which would imply a quadratic complexity growth in the size of the map) by marginalizing out the landmark from each (bundled) measurement. As required for local optimization, we provide a convenient recipe for the gradient of the resulting information matrix Λ in Section 4.
- **Handling many landmarks:** In Section 6 we identify a broad class of observation models for which the contributions from multiple landmarks (accounting for field-of-view) can be compactly evaluated all together. This makes evaluation of a proposed trajectory largely invariant of the number of landmarks, facilitating efficient optimization even when reasoning against large clouds of landmarks. As compared to [23], which only applies to a particular observation and visibility model of *known* landmarks, our decomposition is much more general.

We numerically validate our measurement bundling approximation for both a Dubin’s car and quadrotor systems, demonstrating significant computational improvement with low approximation error. Our full trajectory generation pipeline is evaluated in a large number of random trials for both of these systems, demonstrating better estimation improvement than heuristic methods. Although our implementation is not yet fast enough for real-time operation, the improvements herein suggest that an online solution may be feasible in the near future.

2 Preliminaries

We assume the system state x lies on an n -dimensional manifold X with dynamics given by the stochastic ODE

$$dx(t) = f(x(t), u(t)) dt + G(x(t), u(t)) d\mathbf{w}(t) \in T_{x(t)}X, \quad (1)$$

where $T_x X$ denotes the tangent space of X at the point x . The input u is confined to a set \mathcal{U} , and $\mathbf{w}(\cdot)$ is a standard Brownian noise process. We assume measurements are acquired by a collection of homogeneous sensors

$$dz_i = h(x; \ell_i) dt + d\boldsymbol{\nu}_i \quad \in \mathbb{R}^m, \quad (2)$$

each corrupted by a Brownian process noise $\boldsymbol{\nu}_i$ and parameterized by a latent environmental variable ℓ_i (i.e., a *landmark*). We assume that these measurements are acquired synchronously at a discrete sampling frequency $1/\Delta t$ and are mutually independent. Without loss of generality, each $\boldsymbol{\nu}_i$ is assumed to have identity covariance.

Let $(x(\cdot), u(\cdot))$ define a nominal (noise-free) state/control trajectory pair, that is it obeys $\dot{x} = f(x, u)$.

2.1 Optimal Estimation

When x lies on a Riemannian manifold X (not necessarily a vector space), it is convenient to consider tangent-space perturbations $(\mathbf{x}(t), \mathbf{u}(t)) \in T_x X \times T_u \mathcal{U}$. The small-perturbation dynamics can be approximated by linearizing f and h about (x, u) . This gives a stochastic, linear-time-varying (LTV) system

$$d\mathbf{x}(t) = \left(\mathbf{A}(x(t), u(t)) \mathbf{x}(t) + \mathbf{B}(x(t), u(t)) \mathbf{u}(t) \right) dt + \mathbf{G}(x(t), u(t)) d\mathbf{w}(t) \quad (3a)$$

$$d\mathbf{z}(t) = \mathbf{H}(x(t), \ell_i) \mathbf{x}(t) dt + d\boldsymbol{\nu}_i(t). \quad (3b)$$

A fundamental result of linear systems theory is that the covariance of the optimal unbiased estimator of the LTV system (3) is *independent* of the realization of the random processes. In discrete-time, the covariance evolves deterministically as given by the Extended Kalman Filter (EKF) equations

$$\mathbf{S}_k = \mathbf{P}_k^{-1} + \boldsymbol{\Lambda}_k \quad (4a)$$

$$\mathbf{P}_{k+1} = \mathbf{A}_k \mathbf{S}_k^{-1} \mathbf{A}_k^\top + \mathbf{G}_k \mathbf{G}_k^\top \quad (4b)$$

where $\boldsymbol{\Lambda}_k$ is the Fisher information matrix gained with respect to local state \mathbf{x}_k

$$\boldsymbol{\Lambda}_k = \sum_{i=1}^N \mathbb{1}_{\text{vis}}(x(t_k), \ell_i) \mathbf{H}(x(t_k); \ell_i)^\top \mathbf{H}(x(t_k); \ell_i). \quad (5)$$

where $\mathbb{1}_{\text{vis}}(x, \ell) \in \{0, 1\}$ is a visibility indicator. Note that (4) differs slightly from the standard EKF formulation in that the update occurs *before* the propagation step. This is due to our forthcoming definition of \mathbf{H}_k as describing bundled measurements over the subsequent time interval $[t_k, t_{k+1}]$ (see Section 3).

These equations make explicit the well-known fact that the optimal estimator covariance is a deterministic function of the LTV system (3) and therefore of the nominal trajectory $(x(\cdot), u(\cdot))$. Moreover, if the system Jacobians are smooth functions of (a suitable parameterization of) the nominal trajectory, \mathbf{P}_k will be as well.

2.2 Trajectory Optimization

This paper focuses on a deterministic optimal control problem of the form

$$\begin{aligned} \min_{u(\cdot)} \quad & J_c(u) + \lambda J_{\text{unc}}(u) \\ \text{subject to:} \quad & \dot{x}(t) = f(x(t), u(t)) \quad x(0) = x_0 \\ & u(t) \in \mathcal{U} \quad x(t) \in X_{\text{safe}} \end{aligned} \tag{6}$$

where we have augmented a “conventional” cost functional J_c , representing a min-energy or min-time objective, with an uncertainty penalty J_{unc} .

Note that irrespective of the choice of J_{unc} , the presence of nonlinear dynamics are sufficient to imply that only numeric, local solutions are available in practice. Thus, choice of a non-convex J_{unc} does not usually make (6) fundamentally harder to solve. However, it is critical that J_{unc} be differentiable so that gradient-based methods can still be applied, and that such gradients can be efficiently computed.

2.3 Choices of Uncertainty Metric J_{unc}

A number of choices for the uncertainty term J_{unc} have been proposed, but they generally fall into three main classes. Irrespective of this choice, the goal is to produce a multi-objective optimization which smoothly trades physical trajectory cost (captured by J_c) for estimation performance.

Maximizing landmark visibility A common heuristic in the case of landmark-based estimators (i.e. visual-inertial odometry) is to maximize some visibility metric [6, 13]. While this encourages onboard sensors to be pointed towards informative parts of the environment, it does not explicitly capture the observability properties of the system.

Maximizing the Observability Gramian or Fisher-information From a control-theoretic perspective, [10] and [15] propose maximization of metrics based on the Local Observability Gramian (LOG). The LOG is equivalent to the Fisher information (5) up to a constant scaling. Because $\Lambda \succeq 0$ is singular for trajectories about which the system is locally unobservable, [10] and [15] propose maximization of the smallest eigenvalue $s_1(\Lambda) \geq 0$.

However, there are some challenges to direct maximization. Each row and column of Λ corresponds to a different estimated state variable, and can refer to quantities as varied as positions, velocities, and IMU biases. Maximization of individual sub-matrices (e.g., the position block) as proposed by [15] maintains consistent units of measurement, but is information-theoretically equivalent to *conditioning* on all other states (treating them all as known) and fundamentally neglects key observability properties of the system. Joint maximization, on the other hand, requires some scaling method; two different statistical approaches

are presented in [14, 15]. Ultimately, direct maximization of Λ is a heuristic and, as pointed out by [17], can produce expensive trajectories (with respect to J_c) that yield little improvement in estimation error.

Minimizing posterior covariance Following a number of existing works [16, 19], we propose minimization of the posterior estimator covariance $P(t) \succeq 0$. In contrast to the Fisher information (5), the posterior covariance of the EKF captures both the system dynamics and observation. Furthermore, sub-blocks of P_k represent the *marginal* covariances over those variables, capturing the effects of all other unknown states. Minimization over the trajectory allows the optimization to smoothly trade-off between minimizing uncertainty and conventional planning costs, even to the extent of allowing Λ_k singular at some instances. Moreover, this trade-off naturally takes into account the initial uncertainty P_0 .

In particular, if Y is chosen to select the sub-block of P_k corresponding to the estimated position ${}^w\hat{\mathbf{p}}_k$, then

$$J_{\text{unc}}(u) \triangleq \sum_{k=1}^K \text{tr}(Y P_k Y^\top) = \sum_{k=1}^K \mathbb{E} \| {}^w\hat{\mathbf{p}}_k - {}^w\mathbf{p}_k \|_2^2. \quad (7)$$

That is, this choice of J_{unc} explicitly minimizes the mean-squared estimator error over position (with well-defined units of m^2). In a sense, minimizing the posterior covariance is similar to maximizing Λ , but warped and scaled *correctly* by the dynamics and prior uncertainty of the system.

3 Approximating High-Rate Sensors

For high-rate sensors such as cameras, simulation of the EKF update (and subsequent gradient back-propagation) at measurement rate can be intractable for real-time planning. For this reason, we propose a computationally-efficient method to “bundle” multiple high-rate measurements into a single update. This provides a simplified proxy for the true onboard estimation scheme, facilitating efficient evaluation and optimization of trajectories.

For a given time interval $[t_k, t_{k+1}]$ and uniform sensor period Δt , we seek the aggregate information-to-be-gained with respect to error state $\mathbf{x}_0 \triangleq \mathbf{x}(0)$. Let $T \triangleq t_{k+1} - t_k$ refer to the interval length and for notational simplicity assume $t_k = 0$. Furthermore, we focus here on the case of a single landmark, allowing us to drop the ℓ_i argument with no loss of generality. The information-to-be-gained with respect to error state \mathbf{x}_0 over the interval $[0, T]$ can be written

$$\Lambda = \sum_{s=0}^{M-1} \Phi(t_s)^\top H(x(t_s))^\top H(x(t_s)) \Phi(t_s) \quad (8)$$

where $M \triangleq T/\Delta t$ and $\Phi(t)$ is the transition matrix of the local LTV system (3).

The expression (8) is equivalent to the nonlinear LOG [10, 17] and represents a “bundled” measurement as desired. However, computation requires evaluating (or approximating) $\Phi(t)$ at M points, which is expensive for high-rate sensors.

Instead, we leverage a Taylor-series expansion to produce a constant-time (independent of M) approximation of (8). Let $L_h^{(j)}$ denote the j^{th} Lie derivative of h , and ∇ the partial derivative operator with respect to \mathbf{x}_0 . Then it can directly be seen that

$$\mathbf{H}(x(t))\Phi(t) = \frac{\partial h(x(t))}{\partial \mathbf{x}(t)} \frac{d\mathbf{x}(t)}{d\mathbf{x}_0} = \frac{dh(x(t))}{d\mathbf{x}_0} = \sum_{j=0}^{\infty} \frac{t^j}{j!} \nabla L_h^{(j)}(x(0)). \quad (9)$$

In practice, it is sufficient to compute only the first r such terms, and substituting into (8) yields

$$\begin{aligned} \Lambda &\approx \sum_{s=0}^{M-1} \left(\sum_{i=0}^{r-1} \frac{(t_s)^i}{i!} \nabla L_h^{(i)} \right)^\top \left(\sum_{j=0}^{r-1} \frac{(t_s)^j}{j!} \nabla L_h^{(j)} \right) \\ &= \sum_{i,j=0}^{r-1} \frac{\sum_{s=0}^{M-1} (s\Delta t)^{i+j}}{i!j!} \nabla L_h^{(i)} \top \nabla L_h^{(j)} \\ &= \left[\nabla L_h^{(0)} \top \nabla L_h^{(1)} \top \dots \nabla L_h^{(r-1)} \top \right] (\mathbf{W} \otimes \mathbf{I}_m) \left[\nabla L_h^{(0)} \top \nabla L_h^{(1)} \top \dots \nabla L_h^{(r-1)} \top \right]^\top \end{aligned} \quad (10)$$

where \otimes refers to the Kronecker product and the elements of the $r \times r$ coupling matrix \mathbf{W} are

$$\mathbf{W}_{ij} \triangleq \frac{\sum_{s=0}^{M-1} (s\Delta t)^{i+j}}{i!j!} = \frac{\lambda_{i+j}}{i!j!} (\Delta t)^{i+j}. \quad (11)$$

Note that $\lambda_p \triangleq \sum_{s=0}^{M-1} s^p$ can be pre-computed for each $p \in \{0, 1, \dots, 2(r-1)\}$, as M is constant in most optimization scenarios.

As desired, (10) represents a constant-time-computable approximation of (8). This summation is equivalent to *stacking* the (correlated) Lie-derivative Jacobians $\nabla L_h^{(j)}$, and computing the aggregate noise matrix \mathbf{W} . Crucially, the inclusion of higher-order derivatives often increases the rank of the bundled measurement, capturing the fact that states that are unobservable under a single measurement may become observable over multiple sequential sensor readings.

In contrast to the E²LOG presented by [15], the bundled measurement (10) explicitly approximates a high-rate *discrete*-time sensor (like a camera). Furthermore, unlike [15] we do not seek to maximize this quantity directly.

For convenience in the duration of this paper, \mathbf{H} will denote the *whitened*, bundled Jacobian with rm (rather than m) rows.

$$\mathbf{H} \triangleq (\mathbf{W} \otimes \mathbf{I}_m)^{\frac{1}{2}} \left[\nabla L_h^{(0)} \top \nabla L_h^{(1)} \top \dots \nabla L_h^{(r-1)} \top \right]^\top \quad (12)$$

4 Differentiable Marginalization

From the previous section, we have several methods to approximate the information acquired from a particular state $x \in X$ over the interval $[t_i, t_{i+1}]$. However,

in the case of landmark-based sensing modalities such as visual odometry, the locations of the landmarks themselves are generally unknown *a priori*, and this uncertainty must be captured in the information update in order to correctly model observability. In this section, we assume that a nominal *linearization point* $\ell \in \mathcal{L}$ is available for each landmark – this provides a well-defined Jacobian $H(x; \ell)$. In practice, this assumption can be met by planning against the current map or by a prior distribution as described in Section 6.

Consider a suitable local parameterization $\mathbf{l} \in \mathbb{R}^d$ of the landmark $\ell \in \mathcal{L}$; then the linearized measurement residual can be written

$$\mathbf{r} = H_x \mathbf{x} + H_\ell \mathbf{l} + \boldsymbol{\nu}. \quad (13)$$

Of course, if the error state vector is augmented to include \mathbf{l} , then H can be applied to the update in the usual way. However, this increases the error state dimension by d for each landmark, representing a quadratic growth in the system covariance matrix. This is computationally intractable when the number of landmarks is large. Some approaches, including [15, 23] simply replace $H \leftarrow H_x$, which from an information-theoretic perspective is equivalent to assuming \mathbf{l} exactly known (*conditioning*). While computationally convenient, this fails to correctly reflect the observability of the actual system and when optimized under (6) may not produce well-observable trajectories.

The information-theoretically correct approach is *marginalization*, producing an “equivalent” measurement over \mathbf{x} which accounts for uncertainty over \mathbf{l} . Assuming H_ℓ has dimension $m \times d$ and letting $r = m - d > 0$, [12] showed that choosing $m \times r$ matrix A such that

$$A^\top H_\ell = 0_{r \times d} \quad \text{and} \quad A^\top A = I_r \quad (14)$$

produces the linearly-transformed residual

$$A^\top \mathbf{r} = A^\top H_x \mathbf{x} + A^\top \boldsymbol{\nu} \quad (15)$$

which is clearly independent of \mathbf{l} such that $A^\top H_x$ maintains maximal information over \mathbf{x} . The unitarity constraint in (14) ensures that the resulting marginalized information matrix $H_x^\top A A^\top H_x$ matches the Schur complement of the full information matrix $H^\top H$.

The value of this “null-space trick” [12] is that finding a satisfactory A is efficiently computable via a partial SVD

$$H_\ell = U \begin{bmatrix} \Sigma_1 \\ 0_{r \times d} \end{bmatrix} V^\top \implies A = U \begin{bmatrix} 0_{d \times r} \\ I_r \end{bmatrix} \quad (16)$$

where U, V are square orthogonal matrices of dimension m and d respectively, and $\Sigma_1 \succ 0$ diagonal of dimension d .

In an optimization framework, we need to be able to compute gradients through this marginalization process. While the SVD is differentiable in general [18], we identify a simpler “pseudo-gradient” of A such that the gradient of the resulting marginalized information matrix can be computed via the product rule

$$d(H_x^\top A A^\top H_x) = dH_x^\top A A^\top H_x + H_x^\top A A^\top dH_x + H_x^\top (A dA^\top + dA A^\top) H_x \quad (17)$$

Such a dA $m \times r$ must satisfy differentiated forms of constraints (14)

$$dA^\top H_\ell + A^\top dH_\ell = 0_{r \times d} \quad \text{and} \quad dA^\top A + A^\top dA = 0_{r \times r} \quad (18)$$

It is straightforward to verify that these conditions will be satisfied by any dA such that

$$dA = U \begin{bmatrix} Z_1 \\ Z_2 \end{bmatrix} \quad (19)$$

$$Z_1 = -\Sigma_1^{-1} V^\top dH_\ell^\top A \quad (20)$$

$$Z_2 = -Z_1^\top \quad (\text{skew-symmetric}) \quad (21)$$

where the inverse of diagonal Σ_1 is trivial to compute, and Z_2 can conveniently be taken as $0_{n \times n}$. In practice, this recipe is inexpensive to compute and straightforward to implement.

Note that we assume that H_ℓ is full rank (rank d) in order to ensure Σ_1 definite. The measurement bundling described in Section 3 is often sufficient to satisfy this requirement, as information from multiple observations over the interval $[t_i, t_{i+1}]$ will render H_ℓ full column-rank even when the instantaneous Jacobian block is not (e.g. for vision-based sensors).

5 Modeling Field-of-View

Many real-world sensors, such as cameras, have limited field-of-view. Because landmarks are often distributed non-uniformly, it is important that generated trajectories point sensors towards informative regions of the environment. In the case of quadrotors with body-mounted cameras, several recent methods [6, 13] have shown that explicit optimization of a landmark visibility objective can by itself produce significant estimation improvement.

A fundamental challenge arises from the fact that the indicator $\mathbb{1}_{\text{vis}}(x, \ell)$ used in (5) is not continuous, and therefore not conducive to optimization. Thus, we instead seek a *smooth* $\sigma : X \times \mathcal{L} \mapsto [0, 1]$ which approximates $\mathbb{1}_{\text{vis}}$.

One possible choice well-suited for a pinhole camera model is

$$\sigma(x, \ell) = \begin{cases} \frac{1}{2}(\cos a\theta + 1) & |\theta| < \theta_{\max} \\ 0 & \text{else} \end{cases} \quad (22)$$

where

$$\theta = \cos^{-1} \left(\frac{{}^c \mathbf{r}^\top \hat{\mathbf{e}}}{\|{}^c \mathbf{r}\|_2} \right) \in [0, \pi] \quad (23)$$

is the angle between the optical axis $\hat{\mathbf{e}}$ and the landmark vector ${}^c \mathbf{r}$ in the camera frame. The scaling parameter can be chosen $a = \pi/\theta_{\max}$, ensuring that σ is continuous and differentiable. Ultimately, the best choice of σ will depend on the choice of sensor model and application. In the case of limited-FoV cameras [13, 23] provide some alternatives, but we found (22) sufficient for our purposes.

6 Handling Many Landmarks

The preceding discussion assumed a generic (albeit sufficiently differentiable) per-landmark observation function $h(x; \ell)$. It would then be expected that at each measurement update timestep, we must in general compute a sum (5) over all N landmarks. Similar in spirit to [23], we would like to identify a class of observation models such that we can “compress” this sum into a (near) constant-time evaluation and eliminate the complexity factor of N .

6.1 A Convenient Class of Measurement Models

Consider the case when there exists a local parameterization of the landmark $\mathbf{l} \in \mathbb{R}^d$ such that the observation function $h(x; \ell)$ is *affine* in the \mathbf{l} . Then h and its Jacobian (even *after* bundling and marginalization) can be written

$$h(x; \ell) = \mathbf{h}_0(x) + \sum_{i=1}^d l_i \mathbf{h}_i(x) \quad (24)$$

$$\mathbf{H}(x; \ell) = \mathbf{H}_0(x) + \sum_{i=1}^d l_i \mathbf{H}_i(x), \quad (25)$$

and (5) will be quadratic in the map $\{\ell^{(n)}\}$ as

$$\begin{aligned} \Lambda(x) = & \sum_{i,j=1}^d \mathbf{H}_i(x)^\top \mathbf{H}_j(x) \underbrace{\left(\sum_{n=1}^N \sigma(x, \ell^{(n)}) l_i^{(n)} l_j^{(n)} \right)}_{\triangleq a_{ij}(x)} \\ & + \sum_{i=1}^d \left(\mathbf{H}_i(x)^\top \mathbf{H}_0(x) + \mathbf{H}_0(x)^\top \mathbf{H}_i(x) \right) \underbrace{\left(\sum_{n=1}^N \sigma(x, \ell^{(n)}) l_i^{(n)} \right)}_{\triangleq b_i(x)} \\ & + \mathbf{H}_0(x)^\top \mathbf{H}_0(x) \underbrace{\left(\sum_{n=1}^N \sigma(x, \ell^{(n)}) \right)}_{\triangleq c(x)}. \end{aligned} \quad (26)$$

From (26), it is clear the landmark dependence is confined to a $d \times d$ matrix $[a_{ij}(x)] \succeq 0$, a length- d vector $b_i(x)$, and a scalar $c(x) \geq 0$. If these “mass coefficients” were computable in constant-time, so would the total information $\Lambda(x)$. Moreover, this decomposition holds for *any* choice of visibility function $\sigma \geq 0$.

Fortunately, there exist useful observation models for which the affine condition (24) is met. In fact, any affine function of the relative landmark position (for example in the vehicle body frame) ${}^b\mathbf{l} = {}^w\mathbf{R}_b^\top ({}^w\mathbf{l} - {}^w\mathbf{p})$ has this property. While this category does *not* include perspective projection, it does include orthographic projection, which has often been used as a proxy [8]. This provides a convenient approximation for visual-SLAM systems, for which observability-based planning has already demonstrated benefit [6, 13, 22].

6.2 Interpretation of the Mass Coefficients

Intuitively, the mass coefficients (a, b, c) represent a visibility-weighted landmark *distribution*, and may be interpreted a number of ways.

An optimized implementation. In problem instances where computing the bundled, marginalized Jacobian $H(x; \ell)$ represents non-trivial computation, (25) allows the linear components to be computed *once* at each evaluation state x_k , and iteration over $\{\ell^{(i)}\}$ can be limited to the computation of (a, b, c) .

Pre-computation and lookup. When σ depends on a low-dimensional component of the state space $y = g(x)$, that is that $\sigma(x, \ell) = \sigma(y, \ell)$, this y -space can be discretized and corresponding values of the mass coefficients can be pre-computed. Then computation can be approximated by a lookup table. For example, the authors of [23] do exactly this for a particular choice of σ , discretizing over a workspace in \mathbb{R}^3 .

A (possibly learned) prior. In many online planning applications, landmarks are discovered and tracked in real-time as they enter the sensor’s FoV. As trajectories are often planned to the edge of (or beyond) the sensing horizon, planning strictly against the *currently*-estimated cloud may lead to myopic, undesirable behaviors such as “turning-back.” This is because the system has no mechanism to anticipate where *new* landmarks may appear. If the coefficients are replaced by suitable *predictive* models (a, b, c) defined solely over X , they can describe a “prior” distribution allowing generalization into unknown space.

7 Experiments

Our approach was implemented on two example domains with limited-FoV orthographic cameras and inertial-measurement units (IMU). The first is a planar Dubin’s car, with a planar camera mounted in the forward, thrusting direction. The second is a quadrotor-based visual-inertial odometry (VIO) system in full 3D, with a forward-mounted camera. The estimation dynamics are

Shared dynamics:

(interpreted in \mathbb{R}^2 or \mathbb{R}^3 ,
respectively)

$${}^w\dot{\mathbf{p}} = {}^w\mathbf{v}$$

$${}^w\dot{\mathbf{v}} = {}^w\hat{\mathbf{a}}$$

$${}^b\dot{\boldsymbol{\omega}} = {}^b\boldsymbol{\alpha}$$

$$u \triangleq ({}^b\boldsymbol{\alpha} \ c)$$

Dubin’s car:

$$x = ({}^w\mathbf{p} \ {}^w\mathbf{v} \ \theta \ \omega \ {}^c\mathbf{R}_b \ {}^c\mathbf{t}_b)$$

$${}^w\hat{\mathbf{a}} = {}^c{}^w\mathbf{R}_b \mathbf{e}_1$$

$$\dot{\theta} = \omega$$

Quadrotor:

$$x = ({}^w\mathbf{p} \ {}^w\mathbf{v} \ {}^w\mathbf{R}_b \ \mathbf{b}_w \ \mathbf{b}_a \ {}^c\mathbf{R}_b \ {}^c\mathbf{t}_b)$$

$${}^w\dot{\mathbf{R}}_b = {}^w\mathbf{R}_b [{}^b\dot{\boldsymbol{\omega}}]_{\times}$$

$${}^b\dot{\boldsymbol{\omega}} = {}^b\boldsymbol{\omega} - \mathbf{b}_\omega$$

$${}^w\hat{\mathbf{a}} = {}^w\mathbf{R}_b ({}^c\mathbf{e}_3 - \mathbf{b}_a) - g\mathbf{e}_3$$

Note that the quadrotor dynamics are IMU-driven, and depend on the unknown bias parameters \mathbf{b}_w and \mathbf{b}_a in \mathbb{R}^3 . Both systems are driven by a commanded

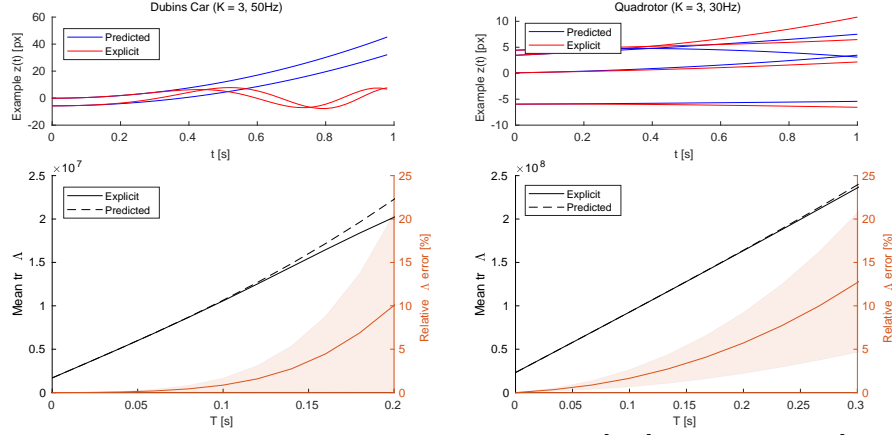


Fig. 1: Sensor approximation results for Dubin's car [left] and quadrotor [right]. The top row shows the measurement evolution of a single random instance of a 2-landmark system. Averaged Λ approximation error over the interval $[0, T]$ is plotted in the bottom row. As expected, error grows with T but remains reasonably small up to moderate time scales.

mass-normalized thrust c and angular acceleration ${}^b\alpha$. The orthographic projection model given landmark ${}^w\mathbf{l}(\ell)$ in \mathbb{R}^2 or \mathbb{R}^3 , respectively, is

$$h(x, \ell) = \mathbf{G}({}^c\mathbf{R}_b {}^w\mathbf{R}_b^\top ({}^w\mathbf{l} - {}^w\mathbf{p}) + {}^c\mathbf{t}_b) \quad (27)$$

where \mathbf{G} is an 1×2 or 2×3 projection matrix $\mathbf{G} = [\mathbf{I} \ \mathbf{0}]$ and the rigid-body transform $({}^c\mathbf{R}_b, {}^c\mathbf{t}_b)$ describes the body-to-camera offset.

7.1 Validation of Measurement Bundling

To evaluate the measurement bundling described in Section 3, we can compare the approximation (10) with the explicit sum (8). For a fixed map of two landmarks in \mathbb{R}^2 or \mathbb{R}^3 , we consider the evolution of the stacked measurement $z(t)$ and the aggregate information Λ over the interval $[0, T]$. The results are plotted in Fig. 1, and show that while error of course grows with time, good approximation ($< 25\%$ error) is achieved for time horizons corresponding to the accumulation of 10 or more measurements in either case. The value of our approximation is demonstrated in Table 1, in which computation time of the full objective are compared with and without our approximation.

7.2 Value of Posterior-Covariance Objective

We compared the performance of the posterior-covariance objective (7) to several heuristics:

Table 1: Timing results on a consumer laptop (includes gradient computation).

System	DOF	K	ΔT	Hz	M	N	Bundling	Avg. eval
Dubin's	9	8	0.25 [s]	50	13	10	Explicit (8)	69.0 [ms]
							Taylor (10)	3.9 [ms]
Quadrotor	21	11	0.15 [s]	30	5	50	Explicit (8)	159.4 [ms]
							Taylor (10)	49.7 [ms]

- **Maximizing landmark visibility:** The method labeled **max-visibility** explicitly maximizes the *total visibility* along the trajectory, using the smooth visibility function given in (22)

$$J_{\text{unc}} \triangleq \sum_{k=1}^K \sum_{n=1}^N \sigma(x(t_k), \ell_n). \quad (28)$$

- **Max Fisher information:** Following [15], **fisher-info** maximizes the smallest eigenvalue of the cumulative Fisher information matrix (5)

$$J_{\text{unc}} \triangleq s_1 \left(\sum_{k=1}^K \mathbf{Y} \Lambda_k \mathbf{Y}^\top \right). \quad (29)$$

Because our sensor model (27) assumes unknown landmarks, absolute position is unobservable and therefore the position sub-matrix of Λ_k is always zero. Therefore we chose \mathbf{Y} to extract the velocity sub-block of Λ_k .

The three methods were evaluated across a batch of 50 random problem instances. In each trial, a random starting state and goal position is selected and a corresponding baseline trajectory is solved for to minimize J_c . Then, this trajectory is refined under the augmented objective (6) via IPOPT [21]. As the weighting parameter λ is increased, the resulting trajectory accepts larger increases in conventional cost J_c for more significant reductions in the uncertainty objective J_{unc} . It is worth noting that while the measurement bundling (10) and smooth FoV (22) approximations may be used during optimization, the output trajectories are evaluated using the explicit measurement rollout (8) and exact visibility indicator $\mathbb{1}_{\text{vis}}(x, \ell)$.

Fig. 2 shows a comparison between the **posterior-cov** objective and various heuristics. The choice of weighting parameter λ defines an effective trade-off between trajectory cost J_c increase and uncertainty reduction (measured as a relative decrease in RMSE). From these results it can be seen that the heuristic objectives do not always produce significant estimation improvement. In comparison, by directly optimizing the posterior-covariance, we obtain larger reductions in RMSE at moderate marginal trajectory cost.

A central goal of observability-based planning is to avoid instances where uncertainty grows to dangerous or catastrophic levels. In Fig. 3 we plot position uncertainties along a large number of simulated trajectories for the two systems. Unrefined trajectories can develop large uncertainty, often well beyond

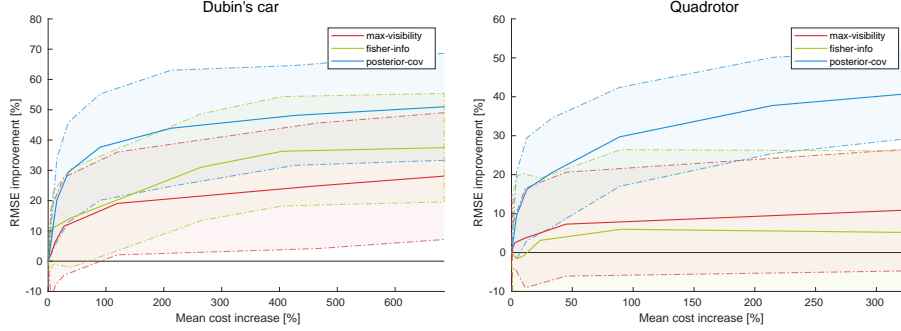


Fig. 2: Each choice of J_{unc} defines an effective trade-off curve between trajectory cost J_c and estimation improvement. We plot this curve by sweeping through the weighting parameter λ and aggregating results for a batch of random trials. Refinement of min-energy trajectories based on heuristic objectives (red, green) does not always yield significant estimation improvement (larger is better). In contrast, minimization of the posterior covariance directly (blue) produces better estimation improvement for the same J_c cost increase.

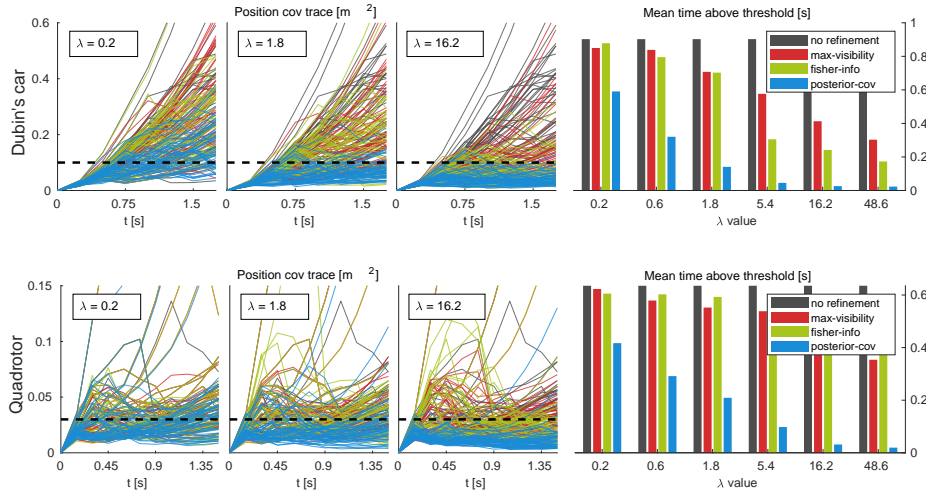


Fig. 3: Evolution of the covariance trace with varying settings of weighting parameter λ (normalized for similar J_c cost increase at given λ). For a chosen “safety” threshold (dashed horizontal line), histograms of expected violation time are shown on the right. Without any refinement (black), uncertainty can grow without bound, but refinement under the **posterior-cov** objective (blue) tends to keep uncertainty bounded, even for relatively low λ . Heuristic (red, green) methods are less effective at ensuring safety.

safe levels, and heuristic refinement methods do not ensure good performance in all instances (even if they do well on average). In contrast, refinement via the `posterior-cov` objective effectively moderates uncertainty growth across a variety of conditions, ensuring safety.

8 Conclusions

Our results indicate that significant estimation improvement can be achieved by explicitly considering observability during trajectory generation. While posterior-covariance minimization is not novel in itself, we address several computational challenges in the case of landmark-based estimators (i.e., visual SLAM). In doing so, we reduce algorithmic complexity from quadratic to linear in the number of landmarks and improve computation in several other ways.

In future work, we hope to produce a real-time implementation capable of online motion planning for a VIO-enabled quadrotor. Furthermore, we plan to explore learned landmark distributions in the context of the quadratic decomposition (26) – that is, learning the mass coefficients a, b, c directly. This would make computation of Λ truly constant-time and enable *anticipation* of new landmarks based on a learned prior. Moreover, it should be possible to approximately extend the decomposition to include perspective projection.

9 Acknowledgment

This work was supported by the Education Office at the Charles Stark Draper Laboratory, Inc. and by ARL DCIST under Cooperative Agreement Number W911NF-17-2-0181.

References

1. Arneberg, J., Tal, E., Karaman, S.: Guidance laws for partially-observable interception based on linear covariance analysis. In: Proc. IEEE Conf. Int. Rob. Sys. (IROS), pp. 4185–4191. IEEE (2018)
2. Bry, A., Roy, N.: Rapidly-exploring random belief trees for motion planning under uncertainty. In: Proc. IEEE Conf. Robot. Autom. (ICRA), pp. 723–730. IEEE (2011)
3. Conticelli, F., Bicchi, A., Balestrino, A.: Observability and nonlinear observers for mobile robot localization. IFAC Proceedings Volumes **33**(27), 663–668 (2000)
4. Elimelech, K., Indelman, V.: Scalable sparsification for efficient decision making under uncertainty in high dimensional state spaces. In: Proc. IEEE Conf. Int. Rob. Sys. (IROS), pp. 5668–5673. IEEE (2017)
5. Elisha, Y.B., Indelman, V.: Active online visual-inertial navigation and sensor calibration via belief space planning and factor graph based incremental smoothing. In: Proc. IEEE Conf. Int. Rob. Sys. (IROS), pp. 2616–2622. IEEE (2017)
6. Falanga, D., Foehn, P., Lu, P., Scaramuzza, D.: PAMPC: Perception-aware MPC for quadrotors. In: Proc. IEEE Conf. Int. Rob. Sys. (IROS), pp. 1–8. IEEE (2018)

7. Indelman, V., Carlone, L., Dellaert, F.: Planning in the continuous domain: A generalized belief space approach for autonomous navigation in unknown environments. *Int. J. of Robotics Research* **34**(7), 849–882 (2015)
8. Kanade, T., Morris, D.D.: Factorization methods for structure from motion. *Philosophical Transactions of the Royal Society of London* **356**(1740), 1153–1173 (1998)
9. Kopitkov, D., Indelman, V.: No belief propagation required: Belief space planning in high-dimensional state spaces via factor graphs, the matrix determinant lemma, and re-use of calculation. *Int. J. of Robotics Research* **36**(10), 1088–1130 (2017)
10. Krener, A.J., Ide, K.: Measures of unobservability. In: *Conf. on Dec. and Control (CDC)*, pp. 6401–6406. IEEE (2009)
11. Mariottini, G.L., Morbidi, F., Prattichizzo, D., Vander Valk, N., Michael, N., Pappas, G., Daniilidis, K.: Vision-based localization for leader–follower formation control. *IEEE Transactions on Robotics* **25**(6), 1431–1438 (2009)
12. Mourikis, A.I., Roumeliotis, S.I.: A multi-state constraint kalman filter for vision-aided inertial navigation. In: *Proc. IEEE Conf. Robot. Autom. (ICRA)*, pp. 3565–3572. IEEE (2007)
13. Murali, V., Spasojevic, I., Guerra, W., Karaman, S.: Perception-aware trajectory generation for aggressive quadrotor flight using differential flatness. In: *American Control Conference (ACC)* (2019)
14. Nobre, F., Heckman, C.: Learning to calibrate: Reinforcement learning for guided calibration of visualinertial rigs. *Int. J. of Robotics Research* (2019)
15. Preiss, J.A., Hausman, K., Sukhatme, G.S., Weiss, S.: Simultaneous self-calibration and navigation using trajectory optimization. *Int. J. of Robotics Research* (2018)
16. Prentice, S., Roy, N.: The belief roadmap: Efficient planning in belief space by factoring the covariance. *Int. J. of Robotics Research* **28**(11-12), 1448–1465 (2009)
17. Raffeisakhaei, M., Chakravorty, S., Kumar, P.: The use of the observability gramian for partially observed path planning problems. pp. 1523–1528. IEEE (2017)
18. Townsend, J.: Differentiating the singular value decomposition. <https://j-towns.github.io/papers/svd-derivative.pdf> (2016). Accessed: 2019-05-14
19. Van Den Berg, J., Abbeel, P., Goldberg, K.: LQG-MP: Optimized path planning for robots with motion uncertainty and imperfect state information. *Int. J. of Robotics Research* **30**(7), 895–913 (2011)
20. Van Den Berg, J., Patil, S., Alterovitz, R.: Motion planning under uncertainty using iterative local optimization in belief space. *Int. J. of Robotics Research* **31**(11), 1263–1278 (2012)
21. Wächter, A., Biegler, L.T.: On the implementation of an interior-point filter line-search algorithm for large-scale nonlinear programming. *Mathematical programming* **106**(1), 25–57 (2006)
22. Zhang, Z., Scaramuzza, D.: Perception-aware receding horizon navigation for MAVs. In: *Proc. IEEE Conf. Robot. Autom. (ICRA)*, pp. 2534–2541. IEEE (2018)
23. Zhang, Z., Scaramuzza, D.: Beyond point clouds: Fisher information field for active visual localization. In: *Proc. IEEE Conf. Robot. Autom. (ICRA)*. IEEE (2019)